Disulfide-Bond Formation in the Transthyretin Mutant Y114C Prevents Amyloid Fibril Formation *in Vivo* and *in Vitro*[†,‡]

Therese Eneqvist,[§,||,⊥] Anders Olofsson,[||,@] Yukio Ando,[#] Taihei Miyakawa,[+] Shoichi Katsuragi,[+] Jana Jass,[@] Erik Lundgren,[@] and A. Elisabeth Sauer-Eriksson*[,§]

Umeå Centre for Molecular Pathogenesis and Department of Molecular Biology, Umeå University, SE-901 87 Umeå, Sweden, and Department of Laboratory Medicine and Department of Psychiatry, Kumamoto University School of Medicine, 1-1-1 Honjo, Kumamoto 860-0811, Japan

Received March 12, 2002; Revised Manuscript Received September 2, 2002

ABSTRACT: The Y114C mutation in human transthyretin (TTR) is associated with a particular form of familial amyloidotic polyneuropathy. We show that vitreous aggregates *ex vivo* consist of either regular amyloid fibrils or disordered disulfide-linked precipitates that maintain the ability to bind Congo red. Furthermore, we demonstrate *in vitro* that the ATTR Y114C mutant exists in three forms: one unstable but nativelike tetrameric form, one highly aggregated form in which a network of disulfide bonds is formed, and one fibrillar form. The disulfide-linked aggregates and the fibrillar form of the mutant can be induced by heat induction under nonreduced and reduced conditions, respectively. Both forms are recognized by the amyloid specific antibody MAB(39−44). In a previous study, we have linked exposure of this epitope in TTR to a three-residue shift in β-strand D. The X-ray crystallographic structure of reduced tetrameric ATTR Y114C shows a structure similar to that of the wild type but with a more buried position of Cys10 and with β-mercaptoethanol associated with Cys114, verifying the strong tendency for this residue to form disulfide bonds. Combined with the *ex vivo* data, our *in vitro* findings suggest that ATTR Y114C can lead to disease either by forming regular unbranched amyloid fibrils or by forming disulfide-linked aggregates that maintain amyloid-like properties but are unable to form regular amyloid fibrils.

Familial amyloidotic polyneuropathy (FAP)[1] is a hereditary form of amyloidosis caused by single-point mutations in the human plasma protein transthyretin (TTR). The clinical manifestation of FAP is peripheral polyneuropathy affecting motor, sensory, and autonomic functions, with accumulation of amyloid deposits mainly along the peripheral nerves, in the kidney, spleen, and heart, and in the intestinal walls (for reviews, see refs *1*−*3*). Currently, more than 70 different single-point mutations are known to cause the disease (see refs *4* and *5* and references therein). In addition, senile systemic amyloidosis (SSA), a condition that affects 25% of the population that is more than 80 years of age, is associated with amyloid deposits in the heart that contain normal and truncated forms of TTR (*6*).

TTR is a 55 kDa protein mainly expressed in the liver, choroid plexus of the brain, and retina. TTR is responsible for distributing the two thyroid hormones triiodothyronine and thyroxine in plasma and cerebrospinal fluid and forms a complex with retinol binding protein (RBP) when the latter is bound to vitamin A (*7*, *8*). The X-ray structure of human TTR was first determined in 1978 but has since then been subjected to several additional structural studies at higher resolution (*9*−*11*). Each monomer comprises a β-barrel formed by two β-sheets (comprising β-strands D, A, G, and H and C, B, E, and F). Dimerization occurs predominantly through an intermolecular main chain interaction between β-strand H of each monomer, forming a continuous eight-stranded β-sheet (Figure 1A). The tetramer forms through hydrophobic interactions between two dimers, thereby creating a central channel with two hormone binding sites (Figure 1B).

A useful tool for studying TTR amyloidosis is available in the form of two monoclonal antibodies, MAB(39−44) and MAB(56−61) (*12*). The highly amyloidogenic transthyretin mutants ATTR G53S/E54D/L55S and ATTR Δ53−55 (*13*), with a substitution or a deletion in the D strand, were used to isolate these antibodies that react specifically with epitopes

[†] Supported by a grant (K2001-03X-13001-03A) from the Swedish Science Council to A.E.S.-E., Lennanders Foundation, and patient associations FAMY and AMYL.

[‡] Atomic coordinates have been deposited in the Research Collaboratory for Structural Bioinformatics (RCSB) as entries 1iii [ATTR Y114C (I)] and 1iik [ATTR Y114C (II)].

* To whom correspondence should be addressed. E-mail: liz@ucmp.umu.se. Phone: +46-90-7856782. Fax: +46-90-778007.

[§] Umeå Centre for Molecular Pathogenesis, Umeå University.

[||] These authors contributed equally to this work.

[⊥] Present address: Department of Molecular Biology, The Scripps Research Institute, 10550 N. Torrey Pines Rd., La Jolla, CA 92037.

[@] Department of Molecular Biology, Umeå University.

[#] Department of Laboratory Medicine, Kumamoto University School of Medicine.

[+] Department of Psychiatry, Kumamoto University School of Medicine.

[1] Abbreviations: FAP, familial amyloidotic polyneuropathy; TTR, transthyretin; ATTR, amyloid TTR; BME, β-mercaptoethanol; MAB(39−44), amyloid specific monoclonal antibody; SSA, senile systemic amyloidosis; IPTG, isopropyl thiogalactopyranoside; TRIS, tris(hydroxymethyl)aminoethane; PEG, polyethylene glycol; AFM, atomic force microscopy; rms, root-mean-square.

10.1021/bi025800w CCC: $22.00
Published on Web 10/11/2002

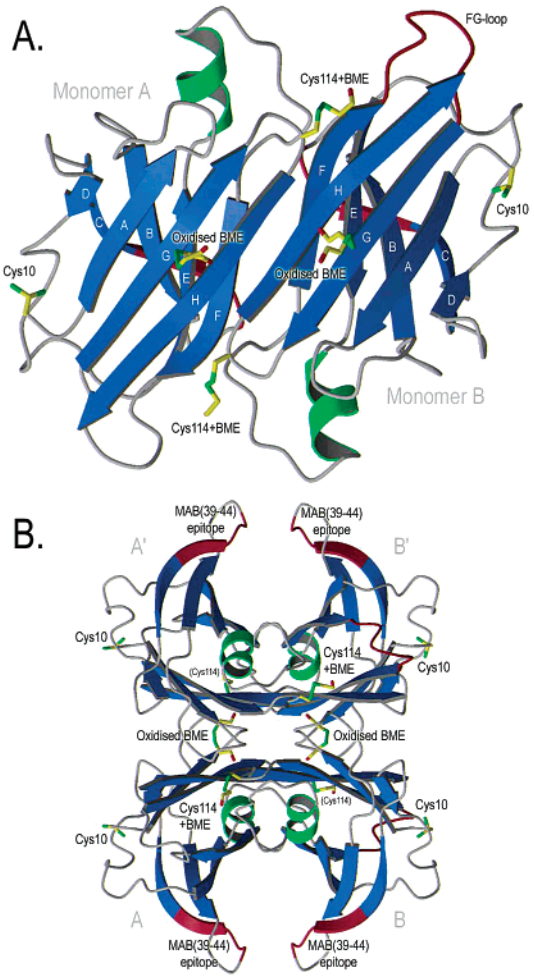

FIGURE 1: Three-dimensional structure of TTR displayed as a (A) dimer and (B) tetramer. The F−G loop in monomer B and the MAB(39−44) epitopes are colored red. The model is drawn from the ATTR Y114C (I) mutant with Cys10, Cys114, and the bound BME molecules shown as sticks. The Cys114 mutation is situated at the G−H loop region right at the dimer−dimer interaction site and at the binding site for RBP (not shown).

exposed in the amyloidogenic conformation and do not recognize TTR variants maintaining the native structure. The X-ray structure of ATTR G53S/E54D/L55S provided detailed information about the nature of the conformational changes at both epitope sites. In particular, the structure showed a conformational rearrangement of the D strand, denoted the β-slip, that provided novel clues to the mechanism of amyloid fibril formation (*14*).

The ATTR Y114C mutation was first described in a Japanese kindred with a particularly severe form of FAP (*15*, *16*), and was later identified also in a Dutch kindred (*17*). The mutant is situated at the G−H loop and provides hydrophobic stabilization of the dimer−dimer packing interactions (Figure 1B). The carriers of this mutation show initial symptoms in their thirties, including vitreous opacities and cardiac involvement, while polyneuropathy is very mild and slowly progressive. Life expectancy is ~10 years after onset of the disease, and the most common cause of death is sudden cardiac malfunction due to heavy amyloid deposits in the heart.

In this study, we have performed a structural and functional characterization of the ATTR Y114C mutant. Electron microscopy studies of *ex vivo* vitreous transthyretin deposits from three ATTR Y114C patients suggest that this mutant forms regular amyloid fibrils or amorphous highly disulfide-linked precipitates without amyloid-like fibrils. We show that ATTR Y114C *in vitro* can by heat induction assemble through intermolecular disulfide bonds into aggregates recognized by MAB(39−44) but with low propensity for amyloid fibril formation. Under reducing conditions, however, fibrillar structures are formed that are recognized by MAB(39−44). This is the first documented case of a TTR mutant that displays two forms of aggregates that share amyloid-like properties such as Congo red staining but with completely different morphologies. In addition, our study links exposure of the epitope recognized by MAB(39−44) to structural changes occurring in a FAP mutant. The X-ray crystallographic structure of reduced ATTR Y114C is very similar to that of wild-type TTR with small conformational changes found only at the position of Cys10. One novel finding is that β-mercaptoethanol binds to the Cys114 residues, hence verifying the strong tendency for this residue to form disulfide bonds.

MATERIALS AND METHODS

Morphological Studies. Vitreous amyloid was collected by centrifugation from three FAP patients carrying the ATTR Y114C mutation: a 44-year-old female with a 6 year duration of disease (patient 1), a 51-year-old female with an 8 year duration of disease (patient 2), and a 48-year-old female also with an 8 year duration of disease (patient 3). The deposits were immersed in 3% glutaraldehyde in phosphate buffer (pH 7.4) for 2 h. After being washed in phosphate buffer for 10 min, the material was immersed in 2.5% osmium tetraxide in phosphate buffer for 2 h, then dehydrated with ethanol, and embedded in Epon. Thick sections were stained with hematoxylin-eosin and Congo red and used for polarized light microscopy (*18*), while thin sections, 25−30 nm, were stained with uranyl acetate and lead acetate before examination with an accelerated voltage of 100 kV in a JEOL 200EX electron microscope.

In Vitro Mutagenesis. The mutant TTR variant was generated using PCR site-directed mutagenesis. Two overlapping sequences were amplified using oligonucleotides (Life Technologies) containing the desired nucleotide substitution and the flanking regions of the TTR gene as primers. The PCR products were purified on a 1.2% agarose gel (NuSieve GTG) and subsequently isolated directly from the gel using spin columns (GenElute, Amersham). After purification, the overlapping fragments were mixed and used as templates for a second PCR run using primers of the flanking regions of TTR, resulting in the full-length sequence with the introduced mutation. Flanking primers tagged with 5′ *Nde*I and 3′ *Bam*HI sites were 5′-GCG GCA TAT GGG ACC TAC GGG CAC CGG T-3′ and 5′-GCG GGA TCC TTA TTC CTT GGG ATT GGT GAC-3′. For the introduction of cysteine at position 114, the 5′-GCT GAG CCC CTG CTC CTA TTC CAC-3′ and 5′-GTG GAA TAG GAG CAG GGG CTC AGC-3′ primers were used with wild-type TTR cDNA inserted in a pET3a vector (*13*) serving as the template. The PCR product was digested with *Nde*I and *Bam*HI (New England Biolabs), extracted with phenol and chloroform, and precipitated with ethanol before ligation into *Nde*I- and *Bam*HI-digested pET3a vectors (*19*) using T4 ligase (New England Biolabs). Competent *Escherichia coli*

DH5α cells were transformed (*20*) and plated on LB agar plates containing 50 μM ampicillin. The clones were screened by digestion of miniplasmid preparations with *Nde*I and *Bam*HI, followed by separation on a 1% agarose gel (SeaKem GTG). DNA sequencing using an ABI 377 sequencer verified the nucleotide substitution.

Purification of Recombinant ATTR Y114C. Competent *E. coli* BL21 cells were transformed (*20*) and plated onto LB agar plates containing 100 μM carbenicillin. Colonies were harvested and grown at 37 °C in 2×YT medium which included 0.4% glucose. When the OD_{600} reached 0.8, the cells were induced with 0.4 mM isopropyl thiogalactopyranoside (IPTG) for 3 h before being harvested by centrifugation. The cells were resuspended in 50 mM TRIS buffer (pH 7.0) containing 50 mM NaCl, 1 mM PMSF, and 20 mg of lysozyme/g of cell pellet and incubated for 30 min at 4 °C. After lysis, DNAse was added in the presence of Mn^{2+} ions followed by centrifugation at 20000*g* for 20 min. The supernatant was loaded onto a 10% preparative native PAGE system (model 491, Prep Cell, Bio-Rad) using a standard TRIS-glycine running buffer at pH 8.5. This purification method produces high yields of approximately 95% pure protein. ATTR G53S/E54D/L55S was purified as previously described (*12*).

Gel Electrophoresis. Proteins were separated on a 16% polyacrylamide gradient gel with a 4% stacking gel using a constant voltage under native conditions or in the presence of SDS according to the standard Laemmli procedure (*21*). Where indicated, 0.1 M β-mercaptoethanol (BME) was included as a reducing agent. All proteins separated under denaturing conditions were boiled for 10 min in SDS loading buffer prior to application.

Indirect Enzyme-Linked Immunosorbent Assay. Polyclonal rabbit antibody to human TTR (Dako, 1:100 dilution) was coated to a microtiter plate, and unoccupied sites were blocked with 5% skim milk. All wells were incubated with 100 mM BME for 1 h followed by three washes with PBSA containing 0.01% Tween 20. Incubations were performed in that buffer, which was also used for washing between all subsequent steps. The different TTR variants were titrated by serial dilution ranging from 10 to 0.01 μg/mL and incubated for 1 h at room temperature. After being washed, the bound protein was probed with MAB(39−44) at 5 μg/mL for 1 h and then detected with horseradish peroxidase (HRP)-labeled mouse anti-mouse IgG (Dako, 1:2000 dilution) using 1 mg/mL 2,2′-azinobis(3-ethylbenzthiazoline) (ABTS) dissolved in 0.05 M citrate-phosphate buffer (pH 5.2) containing 0.015% H_2O_2. The absorbance was measured at 405 nm.

AFM Studies. The protein was diluted to 0.05 mg/mL with distilled water and applied to freshly cleaved ruby red mica (Goodfellow, Canbridge, U.K.). Samples were allowed to adsorb for 30 s, washed three times with distilled water, and air-dried. The bound material was imaged with a Nanoscope IIIa multimode AFM instrument (Digital Instruments, Santa Barbara, CA) using TappingMode in air. A silicon probe was oscillated at 300−310 kHz, and images were collected at an optimized scan rate corresponding to 1−1.5 Hz. All images were flattened and presented in height mode using Nanoscope software (Digital Instruments).

Crystallization and Data Collection. Crystals were grown to approximately 0.1 mm × 0.1 mm × 0.3 mm in ∼5 days at room temperature using the hanging drop vapor diffusion method (*22*). The ATTR Y114C (I) crystals grew from drops containing 10 μL of 3 mg/mL protein in 50 mM TRIS (pH 7.5) mixed with 2 μL of well solution containing 2 M ammonium sulfate, 100 mM sodium citrate, 2% polyethylene glycol (PEG) 200, and 1% BME. The crystals of ATTR Y114C (II) were derived from drops containing 8 μL of 3 mg/mL protein in 50 mM TRIS (pH 7.5) mixed with 2 μL of well solution containing 36−40% monomethyl ether PEG 550, 100 mM sodium citrate (pH 5.0), 100 mM ammonium sulfate, and 0.1% BME. The ATTR Y114C (I) data set was collected at room temperature, while the data set for ATTR Y114C (II) was collected at 100 K from a crystal supported in a cryo loop (*23*). The data were collected on a MAC Science 2030H double-imaging plate area detector using Cu Kα radiation generated from a Nonius FR 591 fine focus rotating anode generator. Both data sets were processed and scaled with the programs DENZO-SCALEPACK (*24*). Intensities were converted to structure factors and placed on an approximate absolute scale using the programs TRUNCATE and CAD (*25*). Details of the data collection and the quality of the data are shown in Table 1.

Structure Determination and Refinement. Atomic coordinates of wild-type TTR [PDB entry 1F41 (*11*)] were used as a starting model, and the structures were determined using difference Fourier techniques. To follow the progress of refinement, the R_{free} value was monitored from the start, with 10% of the reflections included in the test set (*26*). The structures were refined by alternating positional and individual *B*-factor refinement using REFMAC (*27*) with manual model building using the graphics software package O (*28*). Refinement of occupancies for the BME molecules, the side chain of Cys10 in ATTR Y114C (I), and the creation of *B*-factor and root-mean-square (rms) deviation plots was performed with CNS (*29*). The quality of the final models was evaluated with PROCHECK (*30*). Dimer−dimer interaction areas were estimated with AREAIMOL using a 1.4 Å probe radius (*31*), and rms deviations were calculated using LSQMAN (*32*). The details of the refinement statistics are shown in Table 1. Pictures were generated using the programs MOLSCRIPT (*33*) and Raster3D.

RESULTS

Vitreous Masses from Two ATTR Y114C FAP Patients Consist of Amorphous Aggregates and Not Amyloid Fibrils. Isolated vitreous material from three patients with FAP carrying the ATTR Y114C mutation stained with Congo red and showed birefringence under polarized light (Figure 2A). In two patients, these deposits consist of small granules of aggregated protein without detectable fibril formation when examined by electron microscopy (Figure 2B). In the third ATTR Y114C patient, fibrillar structures of amyloid are embedded in the amorphous vitreous material (Figure 2C). These fibrils are morphologically similar to amyloid from ATTR V30M patients.

To investigate the properties of the vitreous material, equal amounts of the aggregates from patient 1 were subjected to SDS−PAGE analysis in the presence or absence of BME. The samples were analyzed by Western blotting using an anti-TTR polyclonal antibody (Dako) (Figure 2D). The

Table 1: Data Collection, Refinement, and Structural Statistics

	TTR Y114C (I)	TTR Y114C (II)
(A) data collection		
space group	$P2_12_12$	$P2_12_12$
cell dimensions *a*, *b*, *c* (Å)	43.52, 86.11, 65.59	43.29, 85.29, 64.78
resolution (highest-resolution shell) (Å)	20−2.0 (2.07−2.00)	20−2.0 (2.07−2.00)
no. of observations	155823	102762
no. of unique reflections	17049 (1661)	16411 (1560)
completeness (%)	98.5 (97.2)	96.9 (94.8)
$I/\sigma(I)$	8.9 (4.3)	9.5 (4.1)
R_{merge}[a] (%)	9.1 (39.8)	7.7 (27.2)
(B) refinement		
resolution range used in refinement (Å)	19.5−2.0	19.3−2.0
no. of reflections in the working set	15298	14658
no. of reflections in the test set	1721	1649
R-factor[b] for the working set (%)	19.7	19.2
R_{free}[c] for the test set (%)	23.6	23.9
no. of residues included in the model	10−124 (A), 10−124 (B)	10−125 (A), 10−124 (B)
no. of water molecules	141	198
occupancy of BME		
linked to Cys114 A/B	0.3/0.3	0.3/0.6
oxidized form in channel A/B	0.6/0.9	0.6/1.0
mean temperature factor (Å^2)	19.9	16.4
Ramachandran plot (most favored, additional allowed, generously allowed) (%)	91.5, 8.0, 0.5	89.1, 10.9, −
rmsd[d] for bond lengths (Å)	0.008	0.009
rmsd[d] for bond angles (deg)	1.21	1.26
rmsd[d] for torsion angles in period 1 (deg)	3.50	3.90
rmsd[d] for torsion angles in period 3 (deg)	16.8	17.7
(C) structure		
rmsd compared to wild-type TTR A/B[e] (Å)	0.18/0.18	0.17/0.20
rmsd for monomer A vs monomer B[e] (Å)	0.39	0.46
dimer−dimer interface area (Å^2)	2430	2402

[a] $R_{merge} = \sum_h\sum_i|I_{ih} - \langle I_h\rangle|\sum_h\sum_i\langle I_h\rangle$, where $\langle I_h\rangle$ is the mean intensity of the *i* observations of reflection *h*. [b] *R*-factor $= \sum||F_{obs}| - |F_{calc}||/\sum|F_{obs}|$, where $|F_{obs}|$ and $|F_{calc}|$ are the observed and calculated structure factor amplitudes, respectively. Summation includes all reflections used in the refinement. [c] $R_{free} = \sum||F_{obs}| - |F_{calc}||/\sum|F_{obs}|$, evaluated for a randomly chosen subset of 10% of the diffraction data not included in the refinement. [d] Root-mean-square deviation from ideal values. [e] The main chain atoms of residues Cys10−Asn98 and Arg104−Thr123 were used in the calculations.

results show a pattern where large aggregates do not enter the gel without the presence of the reducing agent. The presence of disulfide bonds in the vitreous material is also apparent from the change in migration from the intermolecular cross-linked material in lane 2 to the reduced material in lane 3. However, all the material in lane 3 did not become fully reduced, and high-molecular weight aggregates are still present. This shows that the material also contains other types of cross-links, possibly generated by different covalent modifications (*34*, *35*).

The ATTR Y114C Mutant Can Form Intermolecular Disulfide Bonds in Vitro. We have cloned, expressed, and purified the recombinant mutant ATTR Y114C. The quaternary structure was analyzed with native PAGE and SDS−PAGE and compared to those of the wild type and ATTR G53S/E54D/L55S (Figure 3). We found that the ATTR Y114C mutant associates into normal tetramers, but starts forming aggregates at ≥37 °C. Separated on native PAGE, this aggregated form appears as high-molecular weight polymer bands that barely enter the gel (Figure 3A, lane 5). This behavior is similar to that of the highly amyloidogenic substitution mutant ATTR G53S/E54D/L55S (lane 6) (*13*). In the presence of BME, the reduced form of this material (lane 2) migrates as tetramers that are identical to wild-type TTR (lane 1). ATTR G53S/E54D/L55S, on the other hand, is not affected by the addition of BME (lane 3). This suggests that the high-molecular weight aggregates of ATTR Y114C differ in composition from those of the substitution mutant and that they associate through disulfide bonds.

The purified proteins were also analyzed on 0.1% SDS−PAGE. All protein samples were boiled for 10 min before being loaded. As seen in Figure 3, wild-type TTR migrates as mostly monomers (Figure 3B, lanes 1 and 4), whereas the aggregated form of ATTR Y114C displays a ladder of bands with molecular weights ranging from below tetramer size to large aggregates just entering the gel (Figure 3B, lane 5). These bands contain TTR molecules connected through intermolecular disulfide bonds since this mutant migrates as monomers in the presence of BME (lane 2). ATTR G53S/E54D/L55S dissociates into dimers and monomers, where disulfide bonds between Cys10 residues seem to be responsible for the dimerization. At this low SDS concentration of 0.1%, the unboiled samples of wild-type TTR migrate as tetramers, while nonheated ATTR Y114C dissociates like ATTR G53S/E54D/L55S (*13*) into monomers (data not shown), suggesting that their tetrameric structure is destabilized.

By increasing the temperature (>37 °C) or the induction time, we could increase the level of aggregation to the point where adding BME no longer reduced the material back to the tetrameric form. Aggregation was also achieved if BME was added to the material prior to the prolonged heat treatment. Analyzed with native gel electrophoresis, the nonreduced and reduced material barely enters the gel (Figure 3C). However, visualization using atomic force microscopy (AFM) shows that the reduced ATTR Y114C protein forms fibrillar structures, whereas the nonreduced material forms predominantly amorphous aggregates with a very low fibril

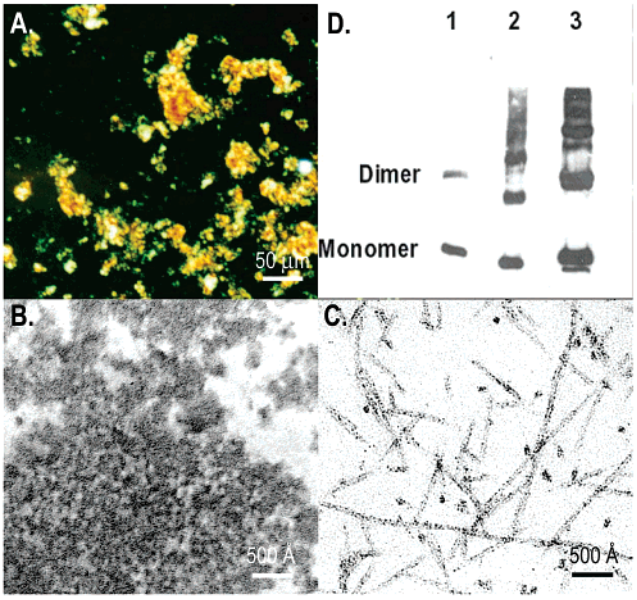

FIGURE 2: Analysis of vitreous deposits isolated from ATTR Y114C FAP patients. (A) Congo red staining from patient 1. (B) Amorphous precipitates from patient 2. (C) Typical amyloid fibrils from patient 3. (D) Western blot on vitreous material isolated from patient 1. The vitreous sample was boiled in SDS for 30 min and divided into two equal halves, and 1% BME was added to one half. Both samples were boiled for an additional 10 min in SDS loading buffer and analyzed using an anti-TTR polyclonal antibody: lane 1, recombinant wtTTR; lane 2, vitreous sample without BME; and lane 3, vitreous sample with BME. A small proportion of wild-type TTR dimers reacts strongly with the polyclonal antibodies (lane 1). The nonreduced vitreous material in lane 2 forms large aggregates that do not enter the gel. The presence of BME reduces these aggregates, leading to an increase in the overall protein concentration in lane 3 compared to that in lane 2. In addition, the presence of BME changes the migration pattern of the vitreous material, showing that it is highly disulfide linked, including also disulfide-linked dimers. The reduced material shows signs of fragmentation, in agreement with results from studies on TTRV30M (*37*).

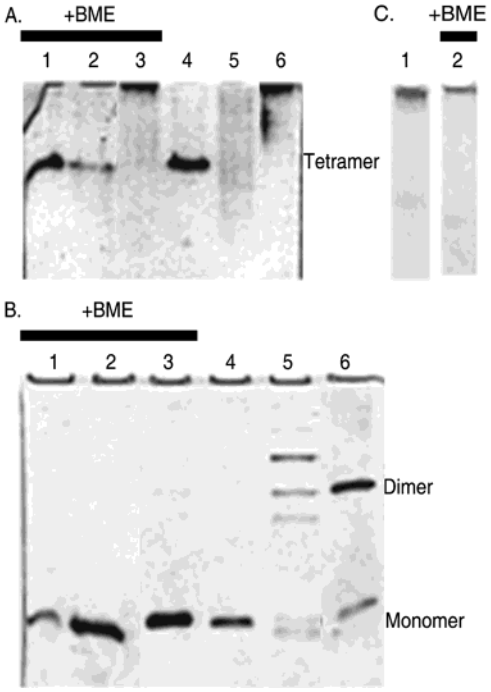

FIGURE 3: Analysis of recombinant TTR under reducing and nonreducing conditions. (A) Native PAGE and (B) 0.1% SDS−PAGE: lanes 1 and 4, wild-type TTR; lanes 2 and 5, ATTR Y114C after heat incubation for 1 day at 37 °C, which induces disulfide-bond formation; and lanes 3 and 6, ATTR G53S/E54D/L55S. (C) Native PAGE of ATTR Y114C after heat induction at 55 °C for 4 days with and without 1% BME. In contrast to the material incubated for 1 day at 37 °C (Figure 3B, lanes 2 and 5), both samples are highly aggregated and barely enter the gel.

content (Figure 4A,B). We typically incubated the samples at 55 °C for 4 days to obtain the fibrils; however, it is likely that other combinations of temperature and induction times will provide the same result.

Disulfide-linked ATTR Y114C Expose Cryptic Epitopes Recognized by MAB(39−44). To probe the conformational changes in the TTR variant under both reducing and nonreducing conditions, we used an indirect enzyme-linked immunosorbent assay (ELISA) with the MAB(39−44) antibody (Figure 5). In the absence of the reducing agent, the antibody reacted strongly toward the disulfide-linked ATTR Y114C aggregates shown in lane 5 of Figure 3, but no reactivity was observed toward the exact same material after reduction with BME to its normal tetrameric form. The reactivity toward the substitution mutant ATTR G53S/E54D/L55S is not affected by the presence of BME. If the ATTR Y114C material were subjected to extensive heat induction (e.g., 4 days at 55 °C), both reduced and nonreduced material is recognized by the antibody (data not shown). As expected, the antibody did not show any reactivity toward the normal wild-type TTR under either condition.

Two Structures of Reduced ATTR Y114C. Two independent structures of ATTR Y114C were refined to 2.0 Å resolution. Structure I was derived from the disulfide-linked material (heated at 37 °C for 1 day) and subsequently reduced to tetramers prior to crystallization. The crystals were grown in ammonium sulfate, and diffraction data were collected at room temperature. The second structure of ATTR Y114C (II) was determined from the nonheated tetrameric form crystallized in PEG using diffraction data collected at ∼100 K. Both crystals belong to space group $P2_12_12$, the same as the majority of the previously determined structures of human TTR (*11*). The structural models maintain good stereochemistry. The data collection and refinement statistics are presented in Table 1.

Both ATTR Y114C structures are very similar to wild-type TTR (Figure 1A). The rms deviations range between 0.17 and 0.20 Å, excluding the N- and C-terminal residues from superposition. This is equivalent to other TTR structures exhibiting the native fold (Table 1). The dimer interface is reduced with areas of 93 (I) and 121 Å^2 (II) compared to the native protein (2523 Å^2). This might be due to the fact that the side chain of Cys is smaller than that of Tyr at position 114 situated in the G−H loop at the dimer−dimer interface (Figure 1B). Nonetheless, these values are still within the normal range for transthyretin structures (*11*).

The two structures of ATTR Y114C are very similar with the only difference being the position of Cys10. In the ATTR Y114C (I) structure, this residue has two rotamers. In one rotamer, the Sγ atom is buried deeper between the main chain oxygens of Leu12 and Leu58. At this position, the Sγ atom prevents water molecule W10 (W12 in monomer B) present in the wild-type structure from binding (Figure 6A). The more buried position of residue 10 in ATTR Y114C (I)

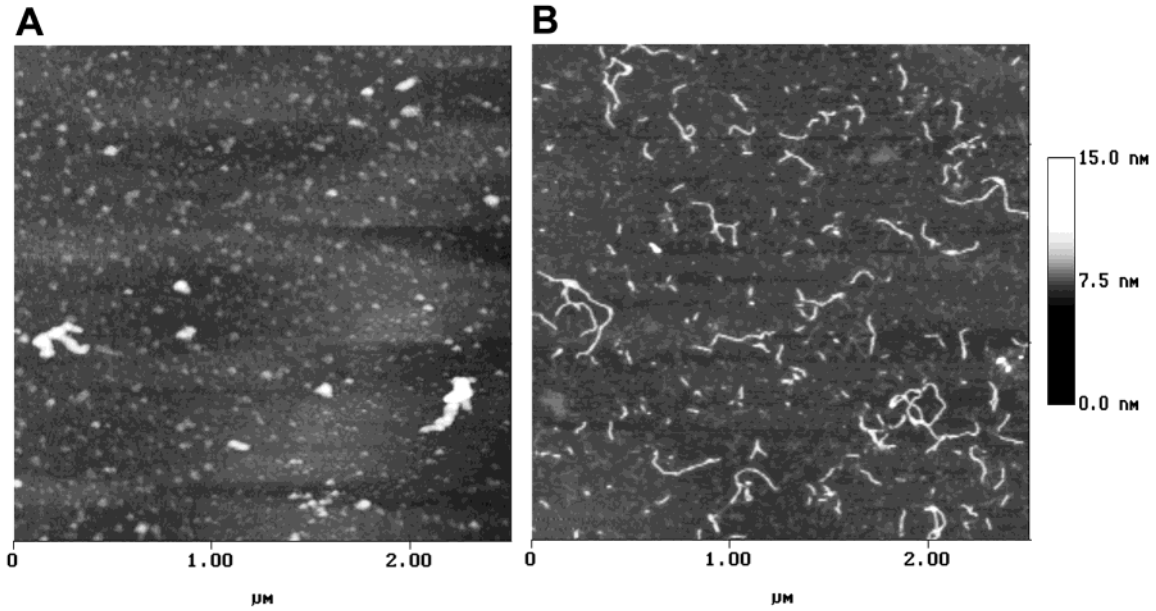

FIGURE 4: Fibrillization studies of recombinant ATTR Y114C material *in vitro*. Equal amounts of protein were incubated at 55 °C for 96 h to induce disulfide-bond formation and fibrillization. Visualization by atomic force microscopy (AFM) of (A) the nonreduced disulfide-linked ATTR Y114C material and (B) the reduced ATTR Y114C material.

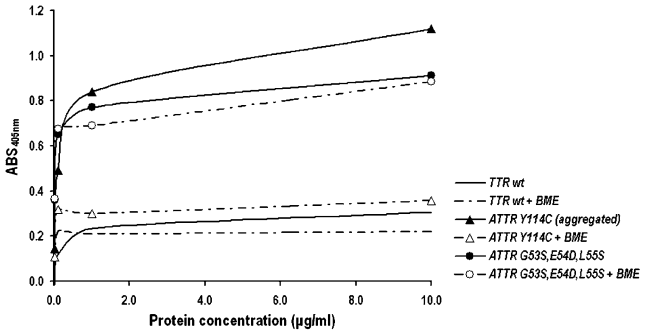

FIGURE 5: Results from an indirect ELISA using MAB(39−44) under nonreducing conditions (−) in the presence of 20 mM BME (− - −). Data for the mutants ATTR Y114C and ATTR G53S/E54D/L55S are shown with triangles and circles, respectively.

causes a minor main chain displacement of 0.5−0.6 Å in the D−E loop which includes His56−Thr65 (Figure 7A). The position of Cys10 in the ATTR Y114C (II) structure resembles that of the wild-type conformation.

The cysteine at position 114 is well-defined in the electron density maps of both structures (Figure 6B). Generally, Cys114 forms a disulfide bond to a BME molecule that occupies roughly the same space as the side chain of the normally occurring tyrosine. The occupancy of this BME molecule varies from 0.3 to 0.6 in the different monomers. The presence of BME affects to some extent the neighboring residues, with minor displacements mainly in the loop following the α-helix in the same monomer and the C-terminal end of the neighboring monomer (Figure 7B).

In the center of the hormone binding channel right at the crystallographic 2-fold symmetry axis, there are two pairs of what appears to be disulfide-linked BME molecules, one in each hormone binding site (Figure 6C). In a test, we replaced the sulfur atoms of the BME molecules with fully occupied water molecules. After refinement, the *B*-factors for these waters were reduced to zero and the distance between them approached 2 Å. This verifies that atoms heavier than oxygen are present at these sites. The oxidized BME molecules replace water molecules W28, W33, W35, and W36. Their hydroxyl groups form hydrogen bonds to the Oγ and Oγ1 atoms of Ser117 and Thr119, respectively. Interestingly, the two oxidized BME molecules are situated right across the hormone binding channel linking the A monomer to its symmetry-related A′ monomer and the B monomer to its symmetry-related B′ monomer (Figure 6C). It is therefore likely that oxidized BME molecules stabilize the tetrameric form of transthyretin. To ensure proper geometry during refinement, two disulfide-linked BME molecules were modeled and refined at each binding site with half-occupancy as included in the deposited coordinates. Generating the tetrameric structure of TTR by applying the 2-fold crystallographic symmetry shows that the two BME molecules in each channel superimposed exactly, which verifies that the four BME molecules bind to the four TTR subunits (A, A′, B, and B′) in exactly the same manner.

DISCUSSION

We demonstrate that vitreous deposits isolated from two ATTR Y114C patients are morphologically different from the fibrillar structures of amyloid found in a third patient. In the former cases, ATTR Y114C forms small granules of amorphous precipitate that stain positively with Congo red, but shows no fibril formation. These patients have symptoms similar to those of the patient with detectable vitreous amyloid, or patients carrying other FAP mutations, including polyneuropathy, vitreous opacities, and cardiac disease (*16*, *17*). High levels of aggregated material are also present in the *ex vivo* material from patients in a Dutch study (*17*). Amorphous material embedded with amyloid fibrils is also found in tissues from ATTR V30M carriers and seems to be composed of several substructures (*36*).

Even though Cys10 is mobile and surface-exposed, disulfide bonds have not been observed between native TTR tetramers. Still, disulfide bonds are present in transthyretin amyloid fibrils (*37*), although they are not a prerequisite for amyloid formation (*38*). Recent findings have shown that

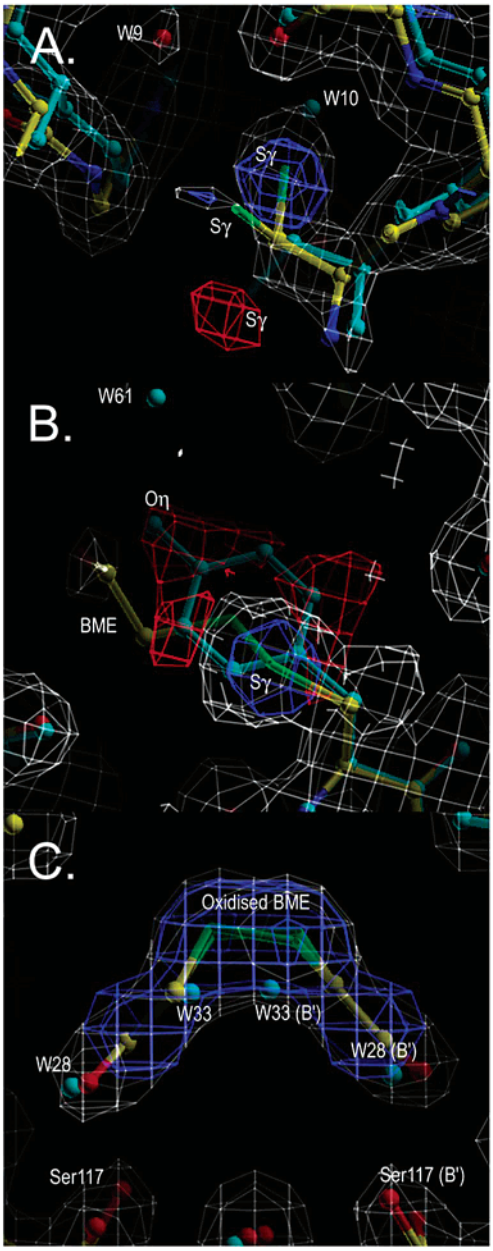

FIGURE 6: Electron density maps from ATTR Y114C (I) visualizing (A) a new conformation of Cys10, (B) the mutation site Cys114, and (C) the oxidized BME in the hormone binding channel. The $2|F_o| - |F_c|$ electron density is contoured at 1σ (light gray) with the side chains of Cys10, Cys114, and the BME molecules omitted from the coordinates before the map calculations. The $|F_o| - |F_c|$ difference electron density map calculated from the wild-type protein coordinates is contoured at 3σ (blue) and -3σ (red) levels. In the latter map, atoms present in the wild-type structure but not in the ATTR Y114C structure appear as negative density (red), whereas atoms present in the ATTR Y114C mutant structure but not in the wild-type structure appear as positive density (blue). Identical atoms at equal positions in both structures are not visible in this type of map. ATTR Y114C (I) is drawn with carbons in yellow, nitrogens in blue, oxygens in red, and sulfurs in green. The wild-type protein is shown in cyan.

the presence of thiol-conjugated TTR in serum (*34*, *35*) and a decreased ratio of unconjugated to conjugated ATTR V30M after onset of disease indicate a propensity for amyloidosis (*34*). The thiol conjugation observed in affected carriers could be a sign of an increasing amount of structurally altered molecules in the serum.

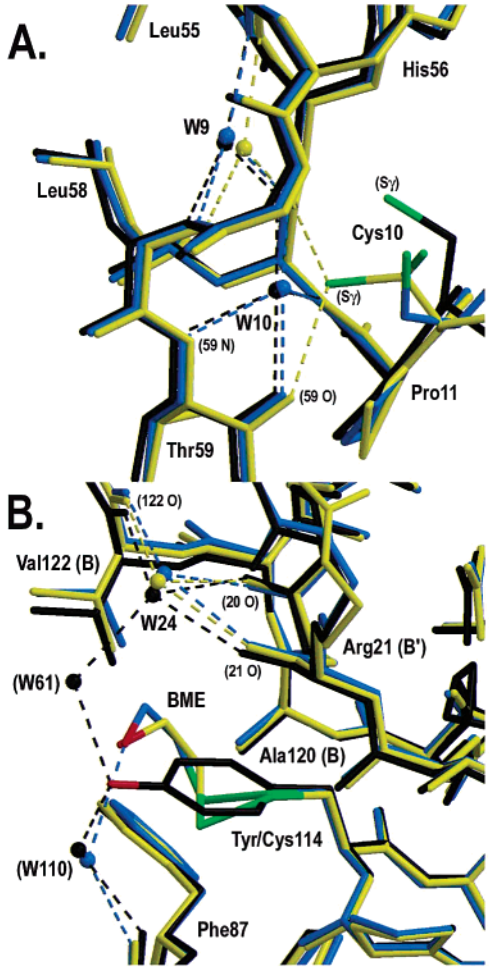

FIGURE 7: Conformational changes present at the two cysteine residues. Structural alignment of ATTR Y114C (I) in yellow, ATTR Y114C (II) in blue, and wild-type TTR (PDB entry 1F41) in black. (A) Cys10 in monomer A. (B) Cys114 in monomer A.

We have analyzed vitreous material of ATTR Y114C with SDS−PAGE under reduced and nonreduced conditions (Figure 2D). The bands migrate differently, indicating the presence of intermolecular disulfide bonds. The amyloidogenic mutant ATTR V30M, however, shows only minor migration differences between reduced and nonreduced vitreous material (*37*). This suggests that the amorphous ATTR Y114C deposits are to a large extent cross-linked through disulfide bonds that are not present in amyloid fibrils. The intra- and intermolecular separations between the Cys10 and Cys114 side chains in the TTR tetramer are greater than 15 Å (Figure 1A,B). This prevents the formation of disulfide bonds both within each monomer and between monomers that are arranged in the regular tetrameric structures (Figure 1B). Disulfide bonds can therefore only be formed between individual monomers, separated dimers, or tetramers. It is not clear if the observed disulfide polymerization involves both Cys10 and Cys114, but given the fact that Cys114 is buried within the tetramer and the evidence from SDS−PAGE, it seems likely that these aggregates contain monomers or dimers linked via both cysteine residues.

Heat induction can be used to generate amyloid fibrils of the wild-type protein (*39*). Increasing the temperature of the recombinant ATTR Y114C protein induces the formation of cysteine-bonded polymers recognized by the amyloid

specific antibody MAB(39−44). The structure of ATTR G53S/E54D/L55S revealed conformational changes that can be associated with amyloid formation (*14*). Protein from dissolved crystals is recognized by MAB(39−44), and compared to the wild type, the structure displays structural differences at the epitope site. It is therefore of interest to draw parallels between this structure and the disulfide-linked form of ATTR Y114C. In ATTR G53S/E54D/L55S, a main chain shift, denoted the β-slip, affects 14 residues (Ser50−Glu63 in the C−D loop, D strand, and D−E loop). This β-slip leads to a three-residue shift in the position of the D strand and facilitates new protein−protein interactions between TTR tetramers. If we assume that the conformational changes at the MAB(39−44) recognition site are induced by the β-slip, we can relate the structural changes observed in the ATTR G53S/E54D/L55S mutant to the ATTR Y114C mutant, which is known to cause FAP. In the ATTR G53S/E54D/L55S structure, the β-slip directly affects the environment of Cys10, which is more mobile than that in the native fold and only visible in the electron density in one of the four monomers. Despite the fact that no Cys10−Cys10 bonds are observed in the crystallographic structure of ATTR G53S/E54D/L55S, the Cys10 residues are in the vicinity of each other (*14*) and the high-molecular weight aggregates formed by ATTR G53S/E54D/L55S seem to contain some portion of disulfide-linked protein (Figure 3).

In an attempt to obtain evidence for misfolding during this structural event, we determined two structures of ATTR Y114C starting from different conditions: one from reduced disulfide-linked material (I) and one from regular tetrameric material that had not formed disulfide bonds (II). Both structures were crystallized in the presence of BME and refined at 2.0 Å resolution. In the ATTR Y114C (I) structure, the side chain of Cys10 occupies a more buried position in the vicinity of the main chain oxygens of Leu12 and Leu58. This is a conformation different from the ATTR Y114C (II) structure and not previously observed in other TTR structures (*11*). Cys10 has been found in several different conformations (*11*); therefore, it is not clear if this new position indicates a significant difference between reduced disulfide-bonded material and normal tetramers, or if it just represents one of a number of possible conformations of Cys10. The novel cysteine residue at position 114 shows a strong tendency to form disulfide bonds being linked to a BME molecule in both structures I and II.

We believe that the high-molecular weight aggregates of ATTR Y114C recognized by MAB(39−44) contain specific structural changes (β-slip-like rearrangements) in addition to the intermolecular disulfide bonds involving Cys10 and Cys114, but that fibril formation itself is prevented by the same cysteine bonds. The amorphous aggregates therefore contain small amyloid-like structures embedded within the disulfide-linked network, which explains the positive birefringence upon Congo red staining. These initially formed oligomeric aggregates can be reversed by adding BME (Figure 5), whereas aggregates generated by prolonged heat incubation are unaffected by the reducing agent. This behavior suggests that covalent bonds are initially formed, which allow an open non-native structure and mediate further aggregation through noncovalent adhesion forces. These forces are, at first, rather weak and are efficiently suppressed by reduction in favor of the more stable tetrameric fold. A prolonged heat incubation, however, mediates an increased level of aggregation that at a certain point renders a structure that is more stable than the native fold. As a result, the tetrameric arrangement can no longer be reversed simply by reduction. This shows that the disulfide-linked network functions as a sterical block within the amyloid maturation process. If the heat incubation is carried out in the presence of reducing agents, fibrils rather than aggregates are formed. The morphology of these fibrillar structures resembles protofibrils, i.e., kinetically trapped intermediate structures of amyloid (Figure 4A,B) (*40*, *41*). In comparison, the ATTR G53S/E54D/L55S mutant binds MAB(39−44) (Figure 5) and forms protofibrils under both nonreduced (*13*) and reduced conditions (data not shown).

Our data suggest that TTR aggregation can follow at least two pathways, amyloid fibril formation or disulfide-bonded polymerization, although the latter seems to be exclusive for TTRs with at least two cysteines per monomer. Both aggregation states bind Congo red, but the symptoms of ATTR Y114C are different from those of other FAP mutations. Most of the patients exhibit vitreous opacity and cardiac disease, whereas sensorimotor polyneuropathy is mild and slowly progressive. Moreover, for ATTR Y114C, leptomeningeal amyloidosis is often recognized. Amorphous material has been observed embedded in amyloid fibrils in peripheral nerves from ATTR V30M carriers (*36*); however, since carrier material normally is not visualized with electron microscopy or AFM, the proportion and significance of its presence for the initiation and progression of the disease are unclear. Cell culture experiments have recently shown that the major toxic effect from TTR correlates with rather early and amorphous aggregates and that the final state represented by amyloid is an inert end state (*42*, *43*). The discovery that ATTR Y114C is prone to aggregation as a function of temperature and that formation of disulfide bridges can inhibit maturation at an intermediate level provides two mechanisms for evaluation of the toxicity of various aggregation forms. We suggest that the interactions of ATTR Y114C disulfide-linked molecules might explain the differences in clinical manifestations and organ distribution of amyloid deposits in these patients.

ACKNOWLEDGMENT

We thank Dr. Uwe H. Sauer for his assistance with X-ray data collection and Terese Bergfors for critical reading of the manuscript.

REFERENCES

1. Benson, M. D., and Uemichi, T. (1996) *Amyloid 3*, 44−56.
2. Saraiva, M. J. (1995) *Hum. Mutat. 5*, 191−196.
3. Hamilton, J. A., and Benson, M. D. (2001) *Cell. Mol. Life Sci. 58*, 1491−1521.
4. Connors, L. H., Richardson, A. M., Théberge, R., and Costello, C. E. (2000) *Amyloid 7*, 54−69.
5. Eneqvist, T., and Sauer-Eriksson, A. E. (2001) *Amyloid 8* (3), 149−168.
6. Westermark, P., Sletten, K., Johansson, B., and Cornwell, G. G. d. (1990) *Proc. Natl. Acad. Sci. U.S.A. 87*, 2843−2845.
7. Schreiber, G., and Richardson, S. J. (1997) *Comp. Biochem. Physiol., Part B: Biochem. Mol. Biol. 116*, 137−160.
8. . Power, D. M., Elias, N. P., Richardson, S. J., Mendes, J., Soares, C. M., and Santos, C. R. (2000) *Gen. Comp. Endocrinol. 119*, 241−255.
9. Blake, C. C., Geisow, M. J., Oatley, S. J., Rérat, B., and Rérat, C. (1978) *J. Mol. Biol. 121*, 339−356.

10. Hamilton, J. A., Steinrauf, L. K., Braden, B. C., Liepnieks, J., Benson, M. D., Holmgren, G., Sandgren, O., and Steen, L. (1993) *J. Biol. Chem. 268*, 2416−2424.
11. Hörnberg, A., Eneqvist, T., Olofsson, A., Lundgren, E., and Sauer-Eriksson, A. E. (2000) *J. Mol. Biol. 302*, 649−669.
12. Goldsteins, G., Persson, H., Andersson, K., Olofsson, A., Dacklin, I., Edvinsson, Å., Saraiva, M. J., and Lundgren, E. (1999) *Proc. Natl. Acad. Sci. U.S.A. 96*, 3108−3113.
13. Goldsteins, G., Andersson, K., Olofsson, A., Dacklin, I., Edvinsson, Å., Baranov, V., Sandgren, O., Thylén, C., Hammarstrom, S., and Lundgren, E. (1997) *Biochemistry 36*, 5346−5352.
14. Eneqvist, T., Andersson, K., Olofsson, A., Lundgren, E., and Sauer-Eriksson, A. E. (2000) *Mol. Cell 6*, 1207−1218.
15. Ueno, S., Uemichi, T., Yorifuji, S., and Tarui, S. (1990) *Biochem. Biophys. Res. Commun. 169*, 143−147.
16. Ueno, S., Fujimura, H., Yorifuji, S., Nakamura, Y., Takahashi, M., Tarui, S., and Yanagihara, T. (1992) *Brain 115*, 1275−1289.
17. Haagsma, E. B., Post, J. G., DeJager, A. E. J., Nikkels, P. G. J., Hamel, B. C. J., and Hazenberg, B. P. C. (1997) *Amyloid 4*, 112−117.
18. Ando, Y., Ando, E., Ohlsson, P. I., Olofsson, A., Sandgren, O., Suhr, O., Terazaki, H., Obayashi, K., Lundgren, E., Ando, M., and Negi, A. (1999) *Amyloid 6*, 119−123.
19. Rosenberg, A., Lade, B. N., Chui, D.-S., Lin, S.-W., Dunn, J. J., and Studier, F. W. (1987) *Gene 56*, 123−135.
20. Hanahan, D. (1983) *J. Mol. Biol. 166*, 557−580.
21. Laemmli, U. K. (1970) *Nature 227*, 680−685.
22. McPherson, A. (1982) *Preparation and Analysis of Protein Crystals*, John Wiley and Sons, New York.
23. Sauer, U. H., and Ceska, T. A. (1997) *J. Appl. Crystallogr. 30*, 71−72.
24. Otwinowski, Z., and Minor, W. (1997) *Methods Enzymol. 276*, 307−326.
25. Collaborative Computational Project, No. 4 (1994) *Acta Crystallogr. D50*, 760−763.
26. Brünger, A. T. (1992) *Nature 355*, 472−474.
27. Murshudov, G. N., Vagin, A. A., and Dodson, E. J. (1997) *Acta Crystallogr. D53*, 240−255.
28. Jones, T. A., Zou, J. Y., Cowan, S. W., and Kjeldgaard, M. (1991) *Acta Crystallogr. A47*, 110−119.
29. Brünger, A. T., Adams, P. D., Clore, G. M., DeLano, W. L., Gros, P., Grosse-Kunstleve, R. W., Jiang, J. S., Kuszewski, J., Nilges, M., Pannu, N. S., Read, R. J., Rice, L. M., Simonson, T., and Warren, G. L. (1998) *Acta Crystallogr. D54*, 905−921.
30. Laskowski, R. A., Moss, D. S., and Thornton, J. M. (1993) *J. Mol. Biol. 231*, 1049−1067.
31. Lee, B., and Richards, F. M. (1971) *J. Mol. Biol. 55*, 379−400.
32. Kleywegt, G. J. (1996) *Acta Crystallogr. D52*, 842−857.
33. Kraulis, P. J. (1991) *J. Appl. Crystallogr. 24*, 946−950.
34. Suhr, O. B., Svendsen, I. H., Ohlsson, P. I., Lendoire, J., Trigo, P., Tashima, K., Ranlov, P. J., and Ando, Y. (1999) *Amyloid 6*, 187−191.
35. Théberge, R., Connors, L., Skinner, M., Skare, J., and Costello, C. E. (1999) *Anal. Chem. 71*, 452−459.
36. Inoue, S., Kuroiwa, M., Saraiva, M. J., Guimaraes, A., and Kisilevsky, R. (1998) *J. Struct. Biol. 124*, 1−12.
37. Thylén, C., Wahlqvist, J., Haettner, E., Sandgren, O., Holmgren, G., and Lundgren, E. (1993) *EMBO J. 12*, 743−748.
38. McCutchen, S. L., and Kelly, J. W. (1993) *Biochem. Biophys. Res. Commun. 197*, 415−421.
39. Chung, C. M., Connors, L. H., Benson, M. D., and Walsh, M. T. (2001) *Amyloid 8*, 75−83.
40. Rochet, J. C., and Lansbury, P. T., Jr. (2000) *Curr. Opin. Struct. Biol. 10*, 60−68.
41. Olofsson, A., Ippel, H. J., Baranov, V., Horstedt, P., Wijmenga, S., and Lundgren, E. (2001) *J. Biol. Chem. 276*, 39592−39599.
42. Sousa, M. M., Cardoso, I., Fernandes, R., Guimaraes, A., and Saraiva, M. J. (2001) *Am. J. Pathol. 159*, 1993−2000.
43. Andersson, K., Olofsson, A., Nielsen, E. H., Svehag, S. E., and Lundgren, E. (2002) *Biochem. Biophys. Res. Commun. 294*, 309−314.

BI025800W